IEEE Access
Multidisciplinary | Rapid Review | Open Access Journal

Received September 4, 2019, accepted September 25, 2019, date of publication October 1, 2019, date of current version October 15, 2019.

Digital Object Identifier 10.1109/ACCESS.2019.2944965

Assessment and Classification of Mental Workload in the Prefrontal Cortex (PFC) Using Fixed-Value Modified Beer-Lambert Law

UMER ASGHER[1], (Member, IEEE), RIAZ AHMAD[1,2], NOMAN NASEER[3], (Senior Member, IEEE), YASAR AYAZ[1,4], (Senior Member, IEEE), MUHAMMAD JAWAD KHAN[1], AND MUHAMMAD KAMAL AMJAD[1]

[1]School of Mechanical and Manufacturing Engineering (SMME), National University of Sciences and Technology (NUST), Islamabad 44000, Pakistan
[2]Directorate of Quality Assurance and International Collaboration, National University of Sciences and Technology (NUST), Islamabad 44000, Pakistan
[3]Department of Mechatronics Engineering, Air University, Islamabad 44200, Pakistan
[4]National Center of Artificial Intelligence (NCAI), Islamabad 44000, Pakistan

Corresponding author: Umer Asgher (umer.asgher@smme.nust.edu.pk)

ABSTRACT Optical-neuro-imaging based functional Near-Infrared Spectroscopy (fNIRS) has been in use for several years in the fields of brain research to measure the functional response of brain activity and apply it in fields such as Neuro-rehabilitation, Brain-Computer Interface (BCI) and Neuroergonomics. In this paper we have enhanced the classification accuracy of a Mental workload task using a novel Fixed-Value Modified Beer-Lambert law (FV-MBLL) method. The hemodynamic changes corresponding to mental workload are measured from the Prefrontal Cortex (PFC) using fNIRS. The concentration changes of oxygenated and deoxygenated hemoglobin (Δc_{HbO} (t) and Δc_{HbR} (t)) of 20 participants are recorded for mental workload and rest. The statistical analysis shows that data obtained from fNIRS is statistically significant with $p < 0.0001$ and t-values > 1.97 at confidence level of 0.95. The Support Vector Machine (SVM) classifier is used to discriminate mental math (coding) task from rest. Four features, namely mean, peak, slope and variance, are calculated on data processed through two different variants of Beer-lambert Law i.e., MBLL and FV-MBLL for tissue blood flow. The optimal combination of the mean and peak values classified by SVM yielded the highest accuracy, 75%. This accuracy is further enhanced using the same feature combination, to 94% when those features are calculated using the novel algorithm FV-MBLL (with its optical density modelled form the first 4 sec stimulus data). The proposed technique can be effectively used with greater accuracies in the application of fNIRS for functional brain imaging and Brain-Machine Interface.

INDEX TERMS Functional near-infrared spectroscopy (fNIRS), modified Beer-Lambert law (MBLL), mental workload (MWL), emotion, prefrontal cortex (PFC), support vector machine (SVM), neuroergonomics.

I. INTRODUCTION

Stress measurement is a key factor in enhancement of efficiency of a task. If the stress of a person can be predicted, the quality of work and health of the person can be improved. The measurement of stress can be done in different ways: some techniques [1]–[3] use facial gestures, some use questioners to assess the stress level, some methods involve recording of respiration and cardiac activity and recent researches use brain signal recording to monitor the stress and anxiety state in the brain. For mental workload monitoring using brain signals, a Brain-Computer Interface (BCI) is used that can translate brain signals into machine commands. Mostly, neuronal signals recorded by electroencephalography (EEG) are used to monitor the cognitive state of the brain. EEG records stress state in the form of passive neuronal activity of the brain. Several EEG researches [4]–[6] have shown that mental workload can be measured from dorsolateral region of the brain. Moreover, the anxiety, fatigue stress can be measured from the same brain regions [7], [8].

In comparison to EEG, functional near-infrared spectroscopy (fNIRS) measures the hemodynamic activity of the brain. fNIRS has a vital role in active BCI where it is able to

The associate editor coordinating the review of this manuscript and approving it for publication was Vishal Srivastava.

decode multiple brain activates for control and rehabilitation of patients. Also, fNIRS is hybridized with other brain imaging modalities (e.g., EEG) to improve the performance of a BCI system [9]–[13]. fNIRS is widely used to monitor cognitive state of a person. Various cognitive studies [14]–[16] have explored the application of fNIRS for measurement of emotions and cognitive processing, especially in the prefrontal cortex (PFC) region. These studies provided insight into the neural mechanisms behind emotional processing in various cognitive functions. Through investigation of NIRS data yields fine, inclusive representations of neural activation as well as assessments of positive, negative, and natural stimuli during emotion processing. Different researchers have studied diverse emotional responses by presenting corresponding pictures as positive, negative and natural stimuli and have analyzed consistent changes in the PFC [17], [18]. One of the important cognitive dimensions linked to emotional processing is mental-workload or mental-task processing [16], [19]. Various fNIRS studies also have been performed in order to measure mental workload under different real-life conditions [20]–[22].

In fNIRS, brain activity is measured as an increase in oxygen consumption and increase in cerebral blood flow due to neuro-vascular coupling. The main light absorbing molecules in brain tissues are the chromophores including oxygenated hemoglobin (HbO), deoxygenated hemoglobin (HbR), water (H_2O) and other cytochromes. Hemoglobin species are the dominant absorbers in NIR window. Brain activity leads to a change in the concentration of HbO and HbR [23], [24]. In Near infra-red spectroscopy (NIRS), NIR light is used to measure the change in concentration of oxygenated haemoglobin (Δc_{HbO} (t)) and deoxygenated haemoglobin (Δc_{HbR} (t)) present in the blood and brain tissues. The mental cognitive states are measured using fNIRS device that directs a NIR light on PFC area and measures Δc_{HbO} (t) and Δc_{HbR} (t) in brain tissues using Modified Beer-Lambert law (MBLL) method. MBLL accounts for properties like NIR light scattering in brain tissues by means of the average value of path length journeyed by NIR photons and the optical density of NIR photon with a concentration of medium - brain tissues [25]–[27]. Mostly, researchers use the difference of the HbO and HbR at every time instant to measure the changes in the blood flow [25], [28], [29]. The drawback here is the small values and abrupt changes in hemodynamic signals that make it difficult to distinguish between the activity and rest states. So, in order to cater this issue, in this study, hemodynamic changes are measured in reference to a fixed value so as to precisely measure these changes and better classify them in BCI applications.

In this study, we have incorporated a novel fixed value approach in the modified Beer-Lambert law to improve the classification accuracy of a mental workload task. This approach uses a reference value of absorbance of the detected light signal to compute difference in optical density in the standard MBLL equation. Since the changes in optical density became more prominent and thus used in accurate classification of different states of neural activity. This reference value of light intensity is different from baseline calculation. In this study, the mental workloads of participants were acquired by fNIRS in the forms of changes in the concentrations of HbO and HbR using the Modified Beer-Lambert law (MBLL) [25], [26], as mentioned below.

$$\begin{bmatrix} \Delta C_{r\_HbO}(t_i) \\ \Delta C_{r\_HbR}(t_i) \end{bmatrix} = \frac{\begin{bmatrix} \alpha_{HbO}(\lambda_1) & \alpha_{HbR}(\lambda_1) \\ \alpha_{HbO}(\lambda_2) & \alpha_{HbR}(\lambda_2) \end{bmatrix}^{-1} \begin{bmatrix} \Delta OD_r(t_i;\lambda_2) \\ \Delta OD_r(t_i;\lambda_2) \end{bmatrix}}{l \times d}$$

where optical properties; α is extinction coefficient of the medium, l is the length of the path covered by the light, $d(\lambda)$ is the differential pathlength factor at wavelength λ and OD is the optical density. Details on MBLL will be covered in next sections.

The complete eight-step system, including experimentation, data acquisition and processing, is shown in Fig. 1. One of the major contributions of this study is the development of a novel variant of MBLL, the Fixed-Value MBLL (FV-MBLL), and its comparison with MBLL for discrimination of mental math (coding) task from rest. In the FV-MBLL, the difference in optical density is calculated in a slightly different manner (the previous value of absorption is kept constant as reference value $I_{ref(\lambda)}$ and is calculated form the first 4 sec stimulus data). The support vector machine (SVM) classifier was used to discriminate mental-workload from rest tasks for both MBLL and FV-MBLL data. The classification accuracies acquired using SVM on FV-MBLL data were significantly higher than those acquired on MBLL data. The results demonstrate the feasibility of using the FV-MBLL for mental-workload discrimination.

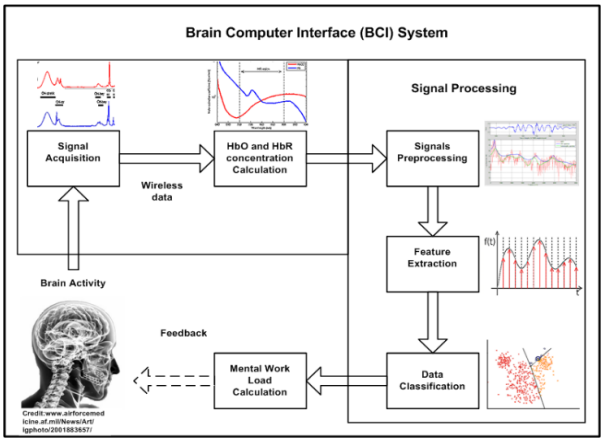

FIGURE 1. fNIRS data acquisition and pre-processing.

II. MATERIALS AND METHODS

A. INSTRUMENTATION AND EXPERIMENTAL SETUP

The fNIRS signals were acquired using a custom-built device "P-fNIRSSys". The fNIRS system (P-fNIRSSyst) used in this study was a continuous-wave (CW) type indigenously developed by our research group working at the School of Mechanical and Manufacturing Engineering (SMME) in the

National University of Sciences and Technology (NUST). This fNIRS system has 12 channels in an array of three dual-wavelength (760 nm and 850 nm) NIR sources and eight detectors, as shown in Figure 2. The emitter-detector distance was set as 2.82 cm in accordance with the literature [30]–[35]. We have compared the mental math results of our machine (P-fNIRSSys) with CW-fNIRS system 'DYNOT-932' from NirX Medical Technologies with sampling rate of 7.94 Hz. Each of the source LEDs consists of two wavelengths but just one of wavelengths (760 nm) of all sources is turned on at one time and then other wavelength (850 nm), so precise switching circuitry was designed to accomplish this task. Circuitry to trigger a particular wavelength of source LED is based on the principle of transistor switching. The detectors were connected in reverse biased configuration. When the light falls on detectors, they conduct and cause current flow that depends upon the intensity of detected light. The analogue pin of the microcontroller is connected to the anode of the photodetector. This voltage is harnessed by the microcontroller using its Analogue to Digital Converter (ADC) module that discretizes the voltage level. Since this voltage level reflects current flow which propositional to the intensity of light reflected, so the detected voltage is proportional of the intensity of reflected light vide Beer's Law [36]. Eight near infrared (NIR) detectors used to detect back reflected radiation. Summing up, in this fNIRS system (P-fNIRSSyst); there are total of 12 channels to be triggered. Each channel consists of a source and a detector as shown in Fig. 2.

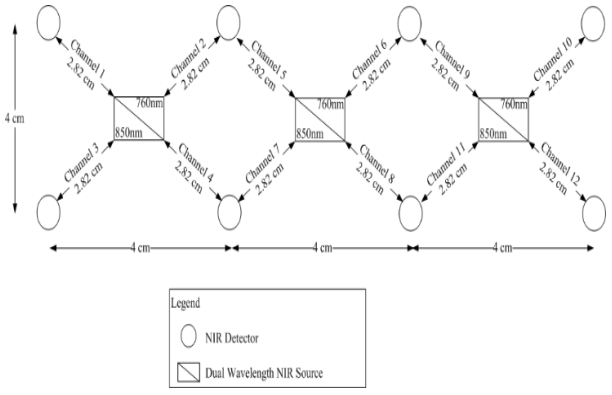

FIGURE 2. Dual-Wavelength fNIRS System (P-fNIRSSyst) with structural mapping of LED sources, detectors and channels positions.

B. DATA ACQUISITION

One 760 nm wavelength in each source (NIR LED) was triggered at a time, and data from the corresponding four channels was acquired. Similarly, the other, 850 nm wavelength was triggered, and again, data from all four corresponding channels was acquired. A delay of 20 ms is introduced between triggering of NIR source wavelength and reading the channels, allowing the NIR source to gain its peak intensity. The process is repeated for all source LEDs and corresponding channels are read. Time of $3\mu s$ is provided for reading the voltage values of the channels. In this study, hemodynamic activity was recorded at a sampling rate of 8 Hz per channel (each wavelength of an LED was triggered eight times per second). The data samples were acquired at all 12 channels as follows:

Total data samples on all 12 channels per second = (12 channels × 8 HbO samples) + (12 channels × 8 HbR samples) equals 192 samples per second. The functional response of the fNIRS system "P-fNIRSSyst" was measured as shown in Fig. 3. This was achieved by presenting the stimulus-response of 25 sec (working-task) to subject 1 at channel 1 and the time course for 25 sec prior to the workload (25 sec) and 15 sec after the stimulus, as shown in Fig. 3. The entire time course of 65 sec was selected in such a manner as to record 520 samples of data (both working memory load and idle state) during that period. Fig. 3 clearly shows that the during the mental activity, the Δ HbO signal state rose in a specific time window of 25 sec with initial dip at the start of activity, and that before and after the activity, we don't have (working-task) signal.

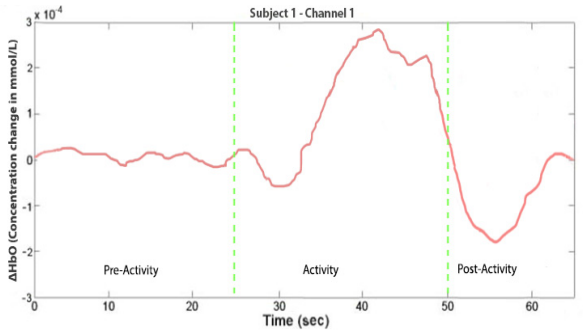

FIGURE 3. fNIRS system (P-fNIRSSyst) functional response, presenting stimulus-response (working-task) in particular time window (25 sec).

Similar results were obtained in various other studies [11], [37], while measuring the function response with fNIRS systems. The results verified that this fNIRS system "P-fNIRSSyst" is capable of measuring real-time functional response. Further, in order to verify the functional-response-measuring capability of the fNIRS system, a similar test was carried out on the rest state alone as well as on mental-workload versus rest data.

C. PARTICIPANTS

Twenty subjects (10 males, 10 females; age range: 20 – 32 years; average age: 28 years) participated in this study. Before final selection, a medical screening interview under the supervision of a medical doctor was conducted in order to reject any prospective participant with any cardiovascular or neurological illness (no participant was rejected). All participants signed a statement of their informed consent to their participation in the study. The participants were given details of the experiment prior to start. All of the experiments were approved by the Ethical Research Council of SMME-NUST and were performed in accordance with the latest Declaration of Helsinki.

D. EXPERIMENTAL PROTOCOL AND MENTAL-WORK LOAD

Participants were briefed about the task in writing and asked for any queries or questions before the start of experiment. In this study, two states were classified to measure improvement in discriminative accuracies. The participants were permitted to write the code in their preferred programming language and were provided a suitable environment in which to concentrate on the task. A visual cue was presented on the screen placed at 70 cm away from the subject. When the cue was given the subject were asked to perform mental math in which the ceil task was used. The cue was given in the form of random numbers displayed on the screen. The sum of the number was greater or less than 743. The subjects were asked to add the random numbers and calculate the sum. If the sum was greater than 743 the subjects were asked to find the value that needs to be subtracted to reach the score of 743. In case the sum was less than 743 the subjects were asked to find the value that needs to be added to reach the score of 743. A total of 5 digits were displayed to estimate the sum. In the last five second the cue was changed and the subjects were asked to think of logic to reach the score using the given number.

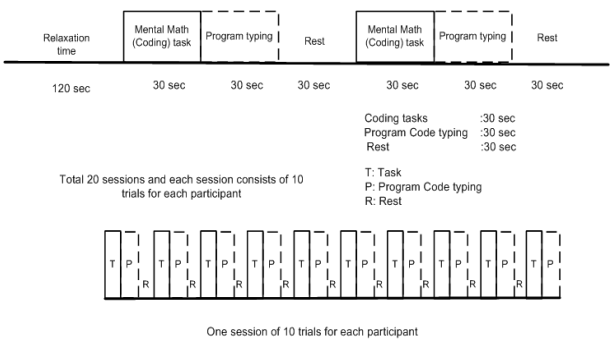

FIGURE 4. Experimental paradigm and data-collection sequence.

The task was composed of both mental math task and mental logic [38]–[42]. The task was selected to evoke the brain activity and entails a certain amount of mental workload, which is prominent is case of mental arithmetic and program coding problems [43]–[45]. The initial two minutes was the rest period, during which the signals could settle to the baseline reference. After the rest period, the participants were asked to perform a 30 sec mental-workload task, which was followed by another 30 sec rest period. The task's duration (30 sec) was selected based on the relevant previous studies [46]–[48]. During rest period, the participants were asked to relax their mind and place mind at rest [39]–[42], [49], [50] so that no brain activity is generated during rest (because focusing on a point or cross, in turns, could generate a brain activity [51], which was not required in this study) and that could be easily differentiated from the mental math task with fNIRS system. This sequence of sessions was repeated ten times (10 trials) for mental task and ten times (10 trials) for rest, for a total of 20 trials for each participant. The signals were recorded in the same sequence with same protocol for all 20 participants as shown in Fig. 4. The total duration of each session consisting 10 trials is 720 seconds per participant and for 20 participants the total experiment time was 14400 sec (240 min). The signal acquired contain artifacts of both high-frequency components such as heartbeat and low-frequency noise due to respiration and Mayer waves [52], [53]. This range of noise components was eliminated by band-pass filtering with a cut-off frequency of 0.1 Hz to 2 Hz.

E. PROPOSED ALGORITHMS: FIXED-VALUE MODIFIED BEER-LAMBERT LAW (FV-MBLL) FOR TISSUE BLOOD FLOW

The MBLL is extensively employed in biophysics and neuro-engineering applications to calculate changes in concentrations of various chromophores present in tissues [36]. The MBLL is a mathematical relationship for computation of Δc_{HbO} (t) and Δc_{HbR} (t) using information on the intensities of detected NIR light at two different time instants [28], [29], [54], [55]. In other words, MBLL relates differential changes in light transmission to differential changes in tissue absorption in brain. Differential changes refer to an assessment between a baseline state and a perturbed state. Absorption is assumed as constant during the measurement and any change in received light is caused by a change in absorption by hemoglobin. fNIRS uses this property of change in received light to calculate a change in concentration of hemoglobin [25], [26], [28]. But this change is relative to a starting-line or baseline. The MBLL equation basically derived from the first order Taylor expansion of the optical density (OD).

$$(OD) = OD^0 + (\partial OD^0/\partial \mu_a)\Delta\mu_a + (\partial OD^0/\partial \mu_s)\Delta\mu_s \quad (1)$$

where OD^0 is the baseline optical density and $\partial \mathrm{OD}/\partial\mu$ is the differential pathlength which is the mean pathlength that diffusing NIR photons travels from source location to the detector. The partial derivatives are evaluated in the baseline state that is $\mu_a^0 = \mu_a$ and $\mu_s^0 = \mu_s$

Thus

$$OD^0 = -\mathrm{Log}[I^0/I^s] \quad (2)$$

where μ_a is the absorption coefficient and μ_s is the scattering coefficient of the medium. The differential changes in absorption $\Delta\mu_a$ and scattering $\Delta\mu_s$ are denoted as:

$$\Delta\mu_a = \mu_a(t) - \mu_a^0 \quad \text{and } \Delta\mu_s = \mu_s(t) - \mu_s^0 \quad (3)$$

The change in optical density w.r.t the baseline and is denoted as

$$\Delta OD = -Log[I(t;\lambda)/I^0] \quad (4)$$

In order to set a baseline I^0, while analyzing data of mental math tasks, the subjects are required to stops their activity (stimuli) during the baseline periods by offering a point to focus so that it will not lead to any extra activity while focusing. The baseline I^0 values are calculated before the activity in the rest period and in some cases after the activity to measure the difference in two base lines I^0 and $\mathrm{I}^{0'}$. According to the

MBLL, the optical density (OD) or absorbance of light (A) is dependent on its wavelength, and is given as:

$$OD(t_i;\lambda) = \mu_a(t_i;\lambda) \times l\mathrm{x}\, d(\lambda) + \eta \tag{5}$$

where $\mu_a(t;\lambda)$ is the absorption coefficient of the medium, l is the length of the path covered by the light, $d(\lambda)$ is the differential pathlength factor, and η is a geometry-dependent factor that accounts for the signal attenuation loss due to scattering. The total attenuation (absorbance/OD) of light of wavelength λ in terms of its detected light intensity $I_{out}(t_i;\lambda)$ or incident intensity $I_{in}(t_i;\lambda)$ is given as:

$$OD(t_i;\lambda) = -\ln \frac{I_{out}(t_i;\lambda)}{I_{in}(\lambda)} \tag{6}$$

In real time data acquisition with CW-fNIRS the light intensities are measured at $1/8^{th}$ (sampling rate) of sec and every time the change in optical density is calculated with reference to previous acquired value. Therefore, change of OD of light may be written as:

$$\begin{aligned}\Delta OD(t_i;\lambda) &= OD(t_i;\lambda) - OD(t_i;\lambda) \\ &= -\ln \frac{I_{out}(t_i;\lambda)}{I_{out}(t_{i-1};\lambda)} = \mu_a(t_i;\lambda) \times l \times d(\lambda)\end{aligned} \tag{7}$$

where $\Delta\mu(t_i;\lambda) = [\alpha_{HbO}(\lambda)\Delta C_{HbO}(t_i) + \alpha_{HbR}(\lambda)\Delta C_{HbR}(t_i)]$

Solving these equations for changes in concentrations $\Delta c_{\mathrm{HbO}}(t_i)$ and $\Delta c_{\mathrm{HbR}}(t_i)$, we obtain:

$$\begin{aligned}\Delta OD(t_i;\lambda) = [&\alpha_{HbO}(\lambda)\Delta C_{HbO}(t_i) \\ &+ \alpha_{HbR}(\lambda)\Delta C_{HbR}(t_i)]\mathrm{x}\, l \times d(\lambda)\end{aligned} \tag{8}$$

Therefore,

$$\begin{bmatrix}\Delta C_{HbO}(t_i) \\ \Delta C_{HbR}(t_i)\end{bmatrix} = \frac{\begin{bmatrix}\alpha_{HbO}(\lambda_1) & \alpha_{HbR}(\lambda_1) \\ \alpha_{HbO}(\lambda_2) & \alpha_{HbR}(\lambda_2)\end{bmatrix}^{-1} \begin{bmatrix}\Delta OD(t_i;\lambda_2) \\ \Delta OD(t_i;\lambda_2)\end{bmatrix}}{l \times d} \tag{9}$$

The MBLL is applied to the raw intensities of detected NIR light, $\Delta c_{\mathrm{HbO}}(t_i)$ and $\Delta c_{\mathrm{HbR}}(t_i)$ are calculated for time instant t_i. It can be seen from equations (7) and (9) that the change in optical density counts for the difference in the intensity of light $I(t_i;\lambda)$ present instant t_i and that of light $I(t_{i-1};\lambda)$ at the previous instant t_{i-1} [25], [28], [29], [55]–[57]. If we fix the value of $I(t_{i-1};\lambda)$ at a reference (value) $I_{ref(\lambda)}$, equations (7) and (9) become:

$$\Delta OD_r(t_i;\lambda) = -\ln \frac{I_{out}(t_i;\lambda)}{I_{ref}} \tag{10}$$

After substituting equation (10) into equation (9), it becomes

$$\begin{bmatrix}\Delta C_{r\_HbO}(t_i) \\ \Delta C_{r\_HbR}(t_i)\end{bmatrix} = \frac{\begin{bmatrix}\alpha_{HbO}(\lambda_1) & \alpha_{HbR}(\lambda_1) \\ \alpha_{HbO}(\lambda_2) & \alpha_{HbR}(\lambda_2)\end{bmatrix}^{-1} \begin{bmatrix}\Delta OD_r(t_i;\lambda_2) \\ \Delta OD_r(t_i;\lambda_2)\end{bmatrix}}{l \times d} \tag{11}$$

where t_i is the present instant of time. The value of $I_{ref(\lambda)}$ is set as the average optical intensity of light under normal conditions for a reference. The reference value $I_{ref(\lambda)}$ is calculated form the first 4 sec activity (stimulus) period data, average it and subtract the average of that from all data points of that trace during activity (stimuli) and similarly for the rest period. Here it is pertinent to mentioned that this reference value $I_{ref(\lambda)}$ is not the baseline I_0 (which has to be calculated before the start of stimuli). $I_{ref(\lambda)}$ is the initial average activity data and used in real time data processing and calculating the real-time differential change in optical density. Now, when we insert these values into equation (9) and find the difference in the OD of light, it comes out as the difference of intensity of light $I(t_i;\lambda)$ at present instant t_i to light intensity $I_{ref(\lambda)}$ at the reference value, as shown in equation (10). Hence, by substituting the value of equation (10) into equation (9), we find the $\Delta c_{\mathrm{HbO}}(t)$ and $\Delta c_{\mathrm{HbR}}(t)$ with respect to the fixed reference value as mentioned in equation (11). New values of change in OD (ΔA_r) are also termed as fixed reference OD. Similarly, the with introduction of ΔA_r in equation (10) the change in concentration of oxygenated ($\Delta C_{r\_HbO}(t_i)$) and deoxygenated hemoglobin $\Delta C_{r\_HbR}(t_i)$ become more prominent. Various research studies on CW fNIRS [25], [49], [58]–[60] have tried similar approaches to calculate improved OD values for taking either the baseline intensity of light *Io(t)* or absolute intensity of light (I_B) to improve measuring ability of the concentration changes. The above-proposed algorithm is termed the Fixed-Value Modified Beer-Lambert Law (FV-MBLL). Using the FV-MBLL, we could achieve better classification accuracies, as will be explained in sections below.

F. FEATURE SELECTION, EXTRACTION AND CLASSIFICATION

In this study, SVM classifiers were used to discriminate mental math (coding) task from rest. SVM has certain advantages over other classifiers, like its flexibility for non-linear classification. Features are calculated for both $\Delta c_{\mathrm{HbO}}(t)$ and $\Delta c_{\mathrm{HbR}}(t)$, and there are different features that can be used for data classification. From various studies [13], [34], [38], [40], [61]–[63], it has been revealed that the maximum accuracy is achieved with mean, peak, slope and variance of $\Delta c_{\mathrm{HbO}}(t)$ and $\Delta c_{\mathrm{HbR}}(t)$ as features. In this study, features were calculated temporarily using a window size of 20 samples (data points) in both workload and rest tasks. They were calculated in consecutive small-time slots of 2.5 sec so as to preserve maximum information in time-series data [64], [65].

The signal mean of $\Delta c_{\mathrm{HbO}}(t)$ and $\Delta c_{\mathrm{HbR}}(t)$ are calculated as:

$$m = \frac{1}{n}\sum\nolimits_{i=1}^{n} X_i \tag{12}$$

where n is the number of observations and Xi represents the $\Delta c_{HbO}(t)$ and $\Delta c_{HbR}(t)$ data. The variance is calculated as:

$$v(X) = \sum (X - \varepsilon)^2/n \tag{13}$$

where ε is the mean value of X. The signal peak value is assessed using the Matlab ''max function''. The signal slope is estimated by fitting a line to all the data points during the mental math task and rest period using polyfit function of Matlab. These features were calculated for the mental math task and rest across 12 channels. So, in order to attain maximum discriminative accuracy between mental-workload and rest tasks, feature combinations are used to ascertain the optimal combination for 4-features data classification [34], [66]. In this study, six different combinations of mean, peak, slope and variance were used for classification: Mean-Variance (M-V), Mean-Peak (M-P), Mean-Slope (M-S), Peak-Slope (P-S), Peak-Variance (P-V), and Slope-Variance (S-V). The objective of SVM is to find the function f (x, w) in the following equation [13];

$$f(x, w) = \vec{w}.\vec{x} + b \tag{14}$$

so as to minimize the objective function;

$$\min J_{\vec{w},\xi}(w, \xi) = \frac{1}{2} \parallel w \parallel + C \sum_{i=1}^{n} \xi n \tag{15}$$

subject to;

$$y_i(\vec{w}.\vec{x} + b) \geq 1 - \xi, \quad \forall i, \xi \geq 0 \tag{16}$$

where the scalar b is the bias, the value of C is maintained at 0.5 so as to avoid either overfitting or underfitting [67], [68], and w is the width of a hyperplane, the objective being to minimize w in order to maximize the SVM accuracy of classification. The hyperplane of SVM demarcates the data sets. In other words, SVM is a mapping function, where data x is input and the data is processed with the help of mapping function f (x, w) in order to obtain output y, which is either $+1$ if the output is greater than 1 or -1 if it is less than -1 [69], [70]. The classification was performed both inter and intra-subject to verify the performance validation of the device and the discriminative accuracies of the FV-MBLL. All machine learning algorithms and data analysis is implemented with the help of Matlab 2018b (MathWorks). In SVM classification, the next step is cross-validation, which is used to calculate classification accuracy. Cross-validation entails segregation of the data samples into subsets and analysis of training and validation data sets. Multiple iterations of cross-validation are executed using different segments or portions to reduce variability, and the results are averaged over all iterations [34], [71], [72]. As a standard, in this study, we used 10-fold cross-validation to compute accuracies for all 12 channels separately against four features in the forms of two-feature combination. In order to calculate the 10-fold cross-validation, the data set was separated into ten subsets, and ten iterations were performed. For each iteration; one of the 10 subsets were used as the test set and the remaining subsets were used as the training sets. The classification accuracy was calculated, and the overall accuracy for all 10 iterations was averaged.

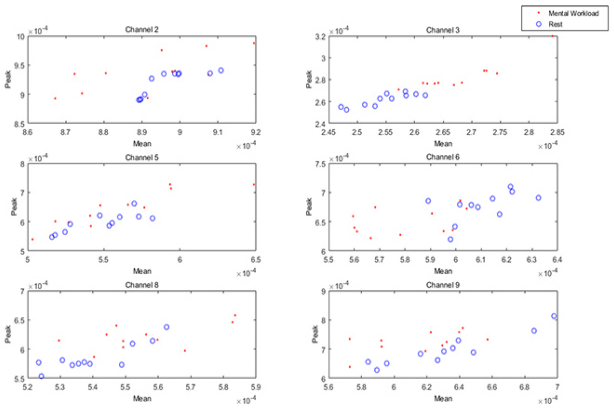

FIGURE 5. Use of MBLL with subject 1's 2-features (mean-peak) combinations in SVM classification for $\Delta c_{HbO}(t)$ at 6 channels sequence.

III. RESULTS

Fig. 5, shows the use of the MBLL with subject 1's 2-feature (mean-peak) combinations for Δc_{HbO} (t) for 20 trials. Similar plots were obtained using subject 1's mean-peak feature combination for Δc_{HbR} (t). Herein, we propose the application of fNIRS for discrimination of the cognitive workload in the PFC from rest tasks. The evidence provided for this application was obtained via fNIRS during 30s mental math task embedded in two rest periods as shown in Table 1. Table 1, shows the quantified average classification and discriminative accuracies achieved for all combinations of 2-dimensional features (mean, peak, slope, and variance) for Δc_{HbO} (t) with both MBLL and FV-MBLL data across all 12 channels for each participant. The individual and average classification accuracies in discriminating the mental-workload tasks and rest activities range from 63 to 74 % in case of MBLL and 80 to 94 % in case of FV-MBLL. Similar results were shown for Δc_{HbR} (t) using both the FV-MBLL and MBLL; however, due to space limitations, only the Δc_{HbO} (t) results were provided. Fig. 6, shows the 2-feature combinations for Δc_{HbO} (t) at 6 channels for 20 trials obtained using the FV-MBLL. For clarity and owning to

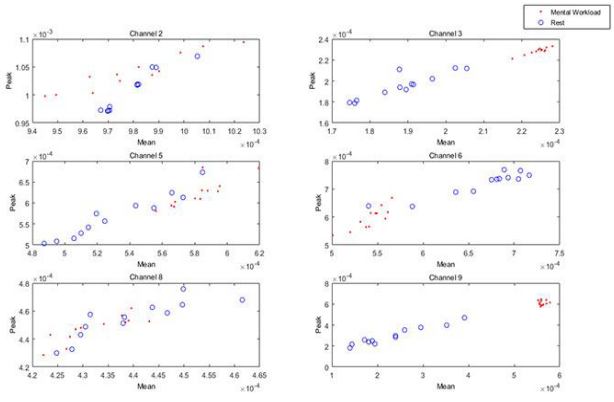

FIGURE 6. 2-Feature (mean-peak) combination in SVM classification plot for $\Delta c_{HbO}(t)$ using FV-MBLL for subject-1 on 6 channels.

TABLE 1. All combinations of 2-dimensional features in SVM for $\Delta c_{HbO}(t)$ by MBLL, FV-MBLL using 10-fold cross-validation.

Feature	Subject 1		Subject 2		Subject 3		Subject 4		Subject 5		Average Accuracy	
	MBLL HbO	FV - MBLL HbO	MBLL HbO	FV - MBLL HbO	MBLL HbO	FV - MBLL HbO	MBLL HbO	FV - MBLL HbO	MBLL HbO	FV - MBLL HbO	MBLL HbO	FV - MBLL HbO
M-P	70	95	75	95	75	90	75	95	75	95	74	94
M-S	65	80	60	80	65	85	65	80	60	80	63	81
M-V	70	85	70	85	65	90	65	80	60	85	66	85
S-P	75	90	70	85	75	85	70	80	85	85	75	85
S-V	65	80	65	80	70	80	65	80	60	85	65	81
P-V	70	95	75	95	70	90	70	90	70	95	71	93
	Subject 6		Subject 7		Subject 8		Subject 9		Subject 10			
M-P	75	95	70	90	75	95	75	95	75	90	74	93
M-S	65	80	65	80	65	80	65	80	65	80	65	80
M-V	70	80	70	80	70	85	70	80	70	85	70	82
S-P	70	85	75	85	75	85	70	85	70	85	72	85
S-V	60	80	70	80	65	80	65	80	65	80	65	80
P-V	75	85	70	95	70	95	70	90	70	85	71	90
	Subject 11		Subject 12		Subject 13		Subject 14		Subject 15			
M-P	75	95	75	90	70	95	70	95	75	95	73	94
M-S	65	80	65	80	60	80	65	90	65	80	64	82
M-V	70	85	70	85	70	85	65	85	70	85	69	85
S-P	70	80	70	90	60	85	60	85	70	80	66	84
S-V	65	80	65	80	65	80	70	80	65	80	66	80
P-V	70	95	70	95	70	95	75	90	70	90	71	93
	Subject 16		Subject 17		Subject 18		Subject 19		Subject 20			
M-P	70	90	70	95	70	95	75	95	75	95	72	94
M-S	65	90	65	80	65	80	65	85	65	80	65	83
M-V	60	80	65	85	70	80	60	80	65	80	64	81
S-P	75	85	70	80	60	90	70	80	70	85	69	84
S-V	65	85	70	85	65	80	60	80	70	80	66	82
P-V	75	95	70	95	75	95	70	90	70	90	72	93

space limitations, only the relevant figures (at 6 channels) are shown; similar figures and tables with results for the other participants on all channels and for other features combinations were omitted.

A. STATISTICAL ANALYSIS OF FNIRS DATA

In this study, in order to gauge the statistical significance of MBLL and FV-MBLL data. Data were analyzed using the software package SPSS Statistics 23 (IBM, Armonk,

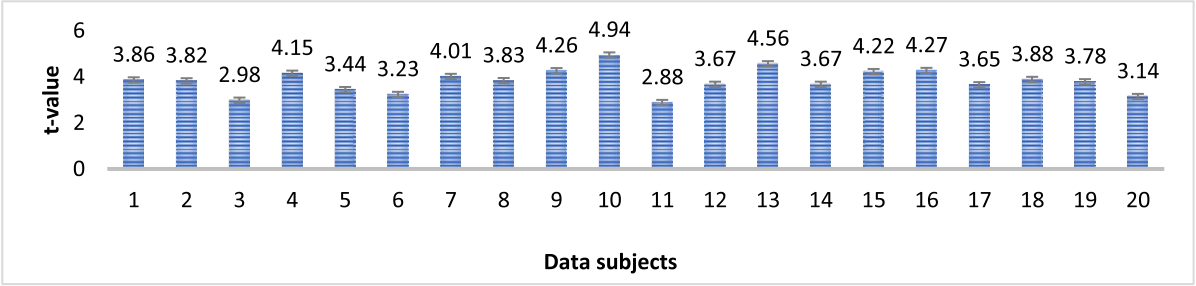

FIGURE 7. t-scores of the data (with p-value < 0.05).

NY, USA). We compared the medians of data sets (MBLL and FV-MBLL). Wilcoxon rank-sum test is used for statistical analysis, two independent data sets (MBLL and FV-MBLL) are considered using null hypothesis and alternative hypothesis. The data's sample size is 1000 both in case of MBLL (n1) and FV-MBLL (n2). For that matter, first we demarcate the hypothesis: In first scenario, null hypothesis (H_0): the two populations (MBLL and FV-MBLL) are equal, there is no significant difference between these two datasets [14], [39], [73] and the p-value is greater than 0.05. Similarly, alternative hypothesis (H_1): the two populations are not equal, a significant difference between two data sets and the p-value is less than 0.05. Two-tailed hypothesis is performed and the p-value comes out to be 0.0001 with a confidence level (α) of 95%. The result is significant with $p < 0.05$ so we reject the null hypothesis-H_o [14], [39]. Similarly, significance of fNIRS data sets is verified by a paired t-test with |t value | > 1.96 (critical value) [75], [76]. The data recorded from all the trials showed a significant *t*-score, as indicated in Fig. 7. *t*-value data of twenty participants' data sets with sequence of ten consecutive trials are presented to validate the findings and accuracies mentioned in Table 1. These *t*-values show an evident significant difference level between the data from two (MBLL and FV-MBLL) populations for 20 subjects.

B. INTER-SUBJECT CLASSIFICATION

The results were interesting when inter-subject classification and validation was measured and calculated for 20 subjects. Inter-subject HbO and HbR data for participants 1-20 were taken and classified using 2 feature combination and 10-fold cross validation as shown in Fig. 8. It shows that the inter-subject classification accuracy is above 80% in all the 2-feature combinations, which is most desirable in most BCI applications [11], [13], [77]. Each participant has an independent feature sign depicted with different colors as shown in the Fig. 8. Subjects are classified based on features against Δc_{HbO} (t) and Δc_{HbR} (t) datasets. The inter-subject classification results show similar patterns in case of optimum classification features Mean-Peak and Peak-Variance combination. Inter-subject classification showed the discriminative average accuracies ranged from 79.75 - 92.12% using FV-MBLL.

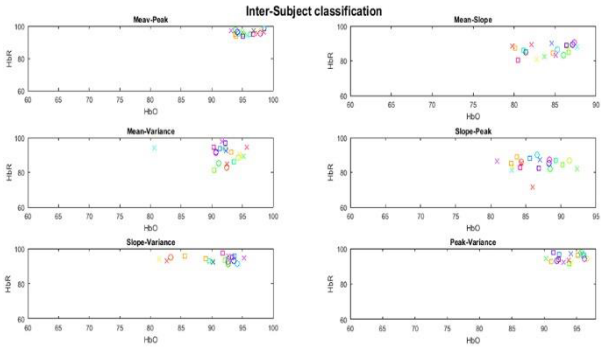

FIGURE 8. Inter-Subject classification and validation for 2-Feature combinations in SVM classification for $\Delta c_{HbO}(t)$ using FV-MBLL.

IV. DISCUSSION

The data from the 20 participants were obtained using, as noted above, the continuous-wave fNIRS system. The changes in concentrations of oxygenated haemoglobin HbO (Δc_{HbO} (t)) and deoxygenated haemoglobin HbR (Δc_{HbR} (t)) were measured using both the MBLL and its variant herein proposed, the FV-MBLL. To measure the significances of those changes and the classification accuracies for the mental-workload and rest tasks, the data was processed with SVM classifiers. The four most commonly used features, ''mean, peak, slope and variance, ''with 2-feature-combination (mean-peak, mean-variance, mean-slope, peak-slope, peak-variance, slope-variance) were selected for measurement of classification accuracies. One-one feature combinations (mean-mean, peak-peak) were used to measure the auto-correlation among the data sets. To be more specific, these discriminative accuracies were extracted from 2-dimensional features derived from Δc_{HbO} (t) and Δc_{HbR} (t) signals. Table 1 shows the discriminative accuracies obtained using the MBLL for (Δc_{HbO} (t)); were within the range of 63– 74% and the discriminative accuracies obtained by applying FV-MBLL on (Δc_{HbO} (t)); were within the 80 - 94% range using all combinations of 2 features in SVM settings. The first-trial experimental results were verified in next ten trials performed on 20 participants in a similar manner, shown in Table 1 for the MBLL and FV-MBLL data sets. Similarly, the accuracies in all the ten trials showing a strong correlation with the discriminative accuracies obtained for each participant with the FV-MBLL data sets. If we summarize the

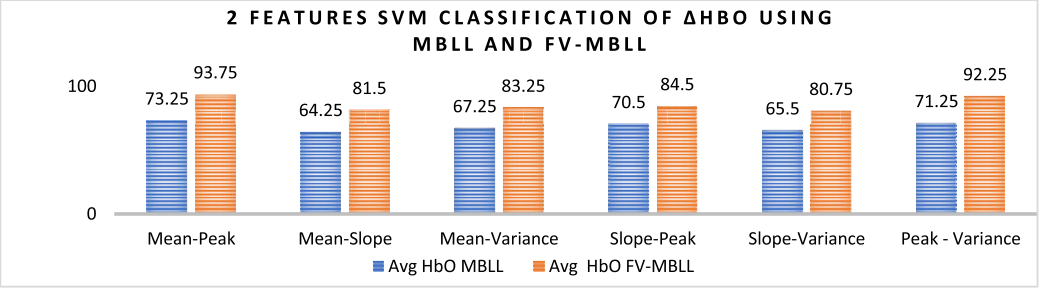

FIGURE 9. Comparison of average accuracies of all 2-Feature combinations in SVM classification for $\Delta c_{HbO}(t)$ using MBLL and FV-MBLL.

findings, the individual (each participant across 12 channels) and average (20 participants with 10 trials of each participant) classification (mental math and rest-task) accuracies with SVM classifiers for the 2-dimensional feature combinations were 68.0 ± 6% in the case of Δc_{HbO} (t), and 67.0 ± 5% in the case of Δc_{HbR} (t) using MBLL data. The individual and average classification accuracies in the case of the FV-MBLL were 87.0 ± 7% for Δc_{HbO} (t), and 85.0 ± 7% for Δc_{HbR} (t) as shown in Table 1. Therefore, a prominent increase of 20% in average classification accuracy was obtained by using the newly proposed FV-MBLL. A comparison among Figs. 5, 6 clearly shows that the Δc_{HbO} (t) and Δc_{HbR} (t) data for the FV-MBLL was more segregated than that obtained with the MBLL. Hence, we can claim that better mental-workload/rest classification accuracies can be achieved using the new FV-MBLL algorithm. The data from the further analyses, shown in Tables 1, Fig. 9 and Fig. 10, indicates that the optimal classification accuracies were obtained with the mean-peak and peak-variance combinations using the MBLL and FV-MBLL as evident in multi-trials results. For analytical convenience and ease of comparison, the discriminative classification data from Tables 1 that shows the average values of classification accuracy for all 2-feature combinations for Δc_{HbO} (t) using both algorithms MBLL and FV-MBLL was summarized in graphical form and complete data findings of Δc_{HbO} (t) and Δc_{HbR} (t).

From Fig. 9, we conclude that classifying mental-math and rest tasks with the SVM classifier using FV-MBLL data in the multi-trial yields the highest classification accuracies up to 93.75%; using the MBLL data meanwhile, the highest classification accuracy was 73.25%, for Δc_{HbO} (t) and the same consistent results were evident after performing ten consecutive trials as shown in Table 1. In order to validate the statistical significance of these SVM classification accuracies, we additionally applied a rank test. The p-values and t-values obtained from the FV-MBLL data versus those from the MBLL data with $p < 0.05$ and $t > 1.96$ for all of the Δc_{HbO} (t) signals and Δc_{HbR} (t) signals, thus establishing the statistical significance [27] of the FV-MBLL's performance as shown in Fig. 7. The combined results plotted in Fig. 10 shows that the mean-peak feature combinations yielded the highest classification accuracies (93.75% for Δc_{HbO} (t) and 90.50% for Δc_{HbR} (t) with FV-MBLL and 73.25% for Δc_{HbO} (t) and 69.50% for Δc_{HbR} (t) with MBLL) and peak-variance (92.25% for Δc_{HbO} (t) and 90.25% for Δc_{HbR} (t) with FV-MBLL and 70.50% for Δc_{HbO} (t) and 71.25% for Δc_{HbR} (t) with MBLL) in all ten trials. The results from the relevant previous studies [34], [38], [61], [62], [71], [78], [79] likewise demonstrate good accuracies (70-90%) for the peak, mean, slope and variance features for both Δc_{HbO} (t) and Δc_{HbR} (t) signals. Various similar studies [33], [34], [37], [63], [78], [80] also shows that combinations of the mean, peak, and variance features achieve the best classification accuracies in mental task/rest discrimination.

Our study also demonstrates the practicability of using those features in combination to attain high discriminative accuracies (up to 94% in multi-trial testing, as noted above).

In our research study, we have 96 data sets in the first trial (48 data sets for MBLL and 48 data sets for FV-MBLL) and same sequence for ten trials, the total data sets come out to be 960 data sets in ten trials setting. The large data sets of twenty participants and multi-trial setup also serve to validate our findings.

Fig. 11, shows the average values of 1-1 feature (mean-mean, peak-peak) combinations in SVM classification and a correlation plot for both Δc_{HbO} (t) and Δc_{HbR} (t) using the MBLL and FV-MBLL. In case of 1-1 feature correlation, the data was highly correlated and that in both cases, the correlation was up to 75.20% for Δc_{HbO} (t) and 76.10% for Δc_{HbR} (t) with MBLL. Similarly, the auto-correlation for the FV-MBLL dataset was as high as 95.40% for Δc_{HbO} (t) and 93.90% for Δc_{HbR} (t) with FV-MBLL. These results verify the significance of the FV-MBLL in that its data more strongly discriminates mental workload than does MBLL data, and to a statistically significant extent. The results for the FV-MBLL data shows that the data's auto-correlation was above 90%; this means that the data set's inter-variance of classification had increased and that the intra-variance of classification had not (the data points of one class were placed very close to each other but far away from the other class's data set). This is the reason that classification/discrimination was easy as compared with the case for MBLL data (the auto-correlation of which was only about 70%). The intra-subject classification was performed to verify the performance validation of the device and the discriminative accuracies of the FV-MBLL as shown in Fig. 6, Fig. 9, Fig. 10 and Table 1. However, the inter subject classification results were promising and data showed similar patterns in case of

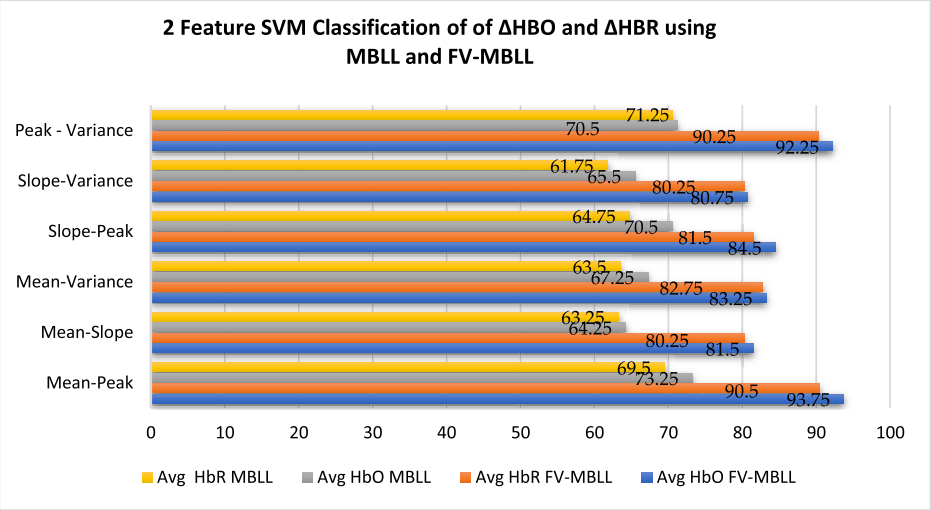

FIGURE 10. Comparison of average accuracies of all 2-Feature combinations in SVM classification for $\Delta c_{HbO}(t)$ and $\Delta c_{HbR}(t)$ using MBLL and FV-MBLL.

Mean-Peak and Peak-Variance combination and were the optimum classification features as shown in Fig. 8. Also, peak was the common feature identified both intra and inter-subject classifications.

Inter-subject classification also showed the better classification accuracies ranged from 79.75 - 92.12% in case of FV-MBLL. These results also validate the intra-subject's FV-MBLL findings.

Different researchers have used different classifiers including LDA, QDA, SVM, KNN, and ANN in discrimination of mental arithmetic and rest tasks [34], [37], [39], [63], [71], [78], [79], the classification accuracies of which ranged from 70 to 85%. The highest average classification accuracies achieved in any of those previous studies for two-class (mental arithmetic and rest task) discrimination was 97.8% using the ANN classifier [63] and 96.3% for 2-feature combinations using the SVM classifier [79], both derived from Δc_{HbO} (t). In our study, in multi-trials settings, for two-class mental-workload task and rest-task discrimination, the average classification accuracies achieved were as high as 93.75% for Δc_{HbO} (t) and 90.50% for Δc_{HbR} (t) using a 2-feature "mean-peak" combination and 92.25% for Δc_{HbO} (t) and 90.25% for Δc_{HbR} (t) using a 2-feature "peak-variance" combination.

The accuracies obtained in this study were analogous to previous highest achieved SVM accuracies; this precision reflects the contribution of the new FV-MBLL algorithm in classification. The comparative histograms in Fig. 10 all shows that the overall classification accuracies obtained using the FV-MBLL were on average 20% higher at all features than those obtained using the MBLL in the paradigm of ten trials. These results support our contention that the FV-MBLL outperforms the conventional MBLL in classification using SVM classifiers. Its performance was further optimized by optimal feature selections, which in our case were the mean-peak and peak-variance feature combinations were the optimal as evident from Table 1, Fig. 9 and Fig. 10. For data acquisition, most of the previous studies [33], [74], [78], [79] have used small sample sizes (5 - 13 participants); in the present study, we compensated for this limitation and validate our findings by implementing a fair sample size (i.e., 20 subjects) with representation of both genders.

The first limitation of this study was the single mental math task and its discrimination from rest. Here, two-state mental workload (mental coding versus rest) are used, whereas varying levels of mental workloads in a more practical way like varying the difficulty level coding problem with varying intensities, could have been considered. The second limitation in our study was that we used only one SVM classifier to measure classification accuracies in discriminating between mental math (coding task) and rest activity. The third limitation was the fact that only four main data features were considered for SVM classification, using 2-feature combinations at a time for classification. In future work, comparison with other classifiers as well as 3-features combination analysis with a wider range (levels) of mental-workloads will further augment the results of this research endeavor.

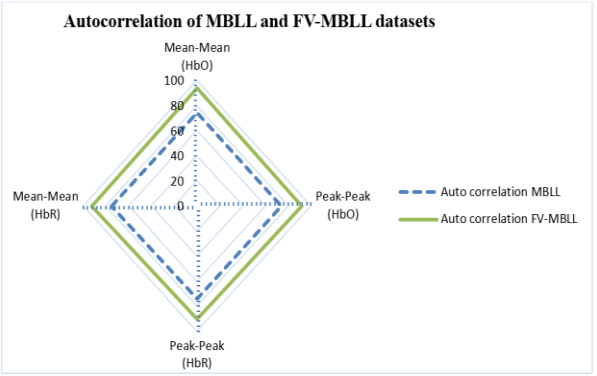

FIGURE 11. Comparison of average accuracies of 1-1 Feature (mean-mean, peak-peak) combinations in SVM classification and autocorrelation plot for $\Delta c_{HbO}(t)$ and $\Delta c_{HbR}(t)$ using MBLL and FV-MBLL.

V. CONCLUSION

In this research, the MBLL (Modified Beer-Lambert Law) and its proposed variant FV-MBLL (Fixed-Value Modified Beer-Lambert Law) were compared for measurement of changes in concentration of oxygenated haemoglobin (Δc_{HbO} (t)) and deoxygenated haemoglobin (Δc_{HbR} (t)) with functional near-infrared spectroscopy (fNIRS) in discriminating mental-workload from rest tasks. The results were investigated with a continues-wave fNIRS system "P-fNIRSSyst" for 2-class mental-workload tasks with a consecutive ten trials setup. Four main data classification features (mean, peak, slope and variance) of the MBLL and FV-MBLL data were used in SVM classifiers to measure the mental-workload / rest-state discriminative accuracies. The significances of the discriminative accuracies were arbitrated across both MBLL and FV-MBLL data sets obtained from 20 participants. We calculated the effects of using different combinations of features for discriminative classification, and for the first time, for measurement of the statistical significance of the results thereby obtained, we investigated 1-1 pair combinations (mean-mean and peak-peak) and determined the autocorrelation with both the MBLL and FV-MBLL data sets using the two-dimensional same-feature-combination technique. We showed that the combination of the peak-mean and variance-peak feature values of Δc_{HbO} (t) and Δc_{HbR} (t) yield the best average classification accuracies, in both participant genders, using both the MBLL and FV-MBLL data sets. The major contribution of this study is its demonstration of the substantially improved SVM classification accuracy (93.75% and 90.50% for Δc_{HbO} (t) and Δc_{HbR} (t), respectively) that is possible with the newly proposed FV-MBLL algorithm (optical density modelled form the first 4 sec stimulus data). The auto-correlation's precision, inter- subject and intra-subject classification accuracies of the FV-MBLL were much superior to those of the MBLL.

CONFLICTS OF INTEREST

The authors declare no conflict of interest.

AUTHORS CONTRIBUTION

Conceptualization, U.A. and N.N.; methodology, U.A. and N.N.; software, U.A and M.J.K.; validation, N.N., Y.A. and M.J.K.; formal analysis, U.A. and M.J.K.; investigation, U.A and M.K.A.; resources, R.A. and Y.A.; writing original draft, U.A.; writing and editing, U.A., M.J.K. and M.K.A; visualization, U.A.,R.A. and M.J.K.; supervision, R.A., N.N and Y.A.; project administration, R.A. and Y.A.

ACKNOWLEDGMENT

The authors would like to acknowledge School of Mechanical and Manufacturing Engineering (SMME), National University of Sciences and Technology (NUST), Islamabad, Pakistan for providing support and opportunity to use facilities and equipment in laboratories for device development, software, data acquisition and analysis. We would also like to specially mention our gratitude to Muhammad Usama, Zargam Ullah, Kashif Ali and Ehtisham ul Hasan for their efforts in initial development of device's hardware and its initial software and special thanks to Khurram Khalil for help in formatting of the article. This research received no external funding.

REFERENCES

[1] C. T. Gloria and M. A. Steinhardt, "Relationships among positive emotions, coping, resilience and mental health," *Stress Health*, vol. 32, no. 2, pp. 145–156, Apr. 2016.
[2] H. Yaribeygi, Y. Panahi, H. Sahraei, T. P. Johnston, and A. Sahebkar, "The impact of stress on body function: A review," *EXCLI J.*, vol. 16, pp. 1057–1072, Jul. 2017.
[3] G. Durantin, J.-F. Gagnon, S. Tremblay, and F. Dehais, "Using near infrared spectroscopy and heart rate variability to detect mental overload," *Behav. Brain Res.*, vol. 259, pp. 16–23, Feb. 2014.
[4] L. Liu, Y. Li, Y. Xiong, J. Cao, and P. Yuan, "An EEG study of the relationship between design problem statements and cognitive behaviors during conceptual design," *Artif. Intell. Eng. Des., Anal. Manuf.*, vol. 32, no. 3, pp. 351–362, Aug. 2018.
[5] W. K. Y. So, S. W. H. Wong, J. N. Mak, and R. H. M. Chan, "An evaluation of mental workload with frontal EEG," *PLoS ONE*, vol. 12, no. 4, Apr. 2017, Art. no. e0174949.
[6] P. Zarjam, J. Epps, and N. H. Lovell, "Beyond subjective self-rating: EEG signal classification of cognitive workload," *IEEETrans. Auton. Mental Develop.*, vol. 7, no. 4, pp. 301–310, Dec. 2015.
[7] F. Al-Shargie, M. Kiguchi, N. Badruddin, S. C. Dass, A. F. M. Hani, and T. B. Tang, "Mental stress assessment using simultaneous measurement of EEG and fNIRS," *Biomed. Opt. Express*, vol. 7, no. 10, pp. 3882–3898, Oct. 2016.
[8] G. Borghini, L. Astolfi, G. Vecchiato, D. Mattia, and F. Babiloni, "Measuring neurophysiological signals in aircraft pilots and car drivers for the assessment of mental workload, fatigue and drowsiness," *Neurosci. Biobehav. Rev.*, vol. 44, pp. 58–75, Jul. 2014.
[9] S. Venclove, A. Daktariunas, and O. Ruksenas, "Functional near-infrared spectroscopy: A continuous wave type based system for human frontal lobe studies," *EXCLI J.*, vol. 14, pp. 1145–1152, Oct. 2015.
[10] M. J. Khan, M. J. Hong, and K.-S. Hong, "Decoding of four movement directions using hybrid NIRS-EEG brain-computer interface," *Frontiers Hum. Neurosci.*, vol. 8, p. 244, Apr. 2014.
[11] K.-S. Hong and M. J. Khan, "Hybrid brain-computer interface techniques for improved classification accuracy and increased number of commands: A review," *Frontiers Neurorobot.*, vol. 11, p. 35, Jul. 2017.
[12] C. A. S. Filho, R. Attux, and G. Castellano, "EEG sensorimotor rhythms' variation and functional connectivity measures during motor imagery: Linear relations and classification approaches," *PeerJ*, vol. 5, p. 3983, Nov. 2017.
[13] S. Ge, Q. Yang, R. Wang, P. Lin, J. Gao, Y. Leng, Y. Yang, and H. Wang, "A brain-computer interface based on a few-channel EEG-fNIRS bimodal system," *IEEE Access*, vol. 5, pp. 208–218, 2017.
[14] F. Al-Shargie, T. B. Tang, and M. Kiguchi, "Stress assessment based on decision fusion of EEG and fNIRS signals," *IEEE Access*, vol. 5, pp. 19889–19896, 2017.
[15] P. H. S. Pelicioni, M. Tijsma, S. R. Lord, and J. Menant, "Prefrontal cortical activation measured by fNIRS during walking: Effects of age, disease and secondary task," *PeerJ*, vol. 7, p. e6833, May 2019.
[16] M. Causse, Z. Chua, V. Peysakhovich, N. Del Campo, and N. Matton, "Mental workload and neural efficiency quantified in the prefrontal cortex using fNIRS," *Sci. Rep.*, vol. 7, Jul. 2017, Art. no. 5222.
[17] Y. Hoshi, J. Huang, S. Kohri, Y. Iguchi, M. Naya, T. Okamoto, and S. Ono, "Recognition of human emotions from cerebral blood flow changes in the frontal region: A study with event-related near-infrared spectroscopy," *J. Neuroimag.*, vol. 21, no. 2, pp. 94–101, Apr. 2011.
[18] H. Doi, S. Nishitani, and K. Shinohara, "NIRS as a tool for assaying emotional function in the prefrontal cortex," *Frontiers Hum. Neurosci.*, vol. 7, no. 2, p. 770, Nov. 2013.
[19] E. Galy, M. Cariou, and C. Mélan, "What is the relationship between mental workload factors and cognitive load types?" *Int. J. Psychophysiol.*, vol. 83, no. 3, pp. 269–275, Mar. 2012.
[20] T. K. K. Ho, J. Gwak, C. M. Park, and J. Song, "Discrimination of mental workload levels from multi-channel fNIRS using deep leaning-based approaches," *IEEE Access*, vol. 7, pp. 24392–24403, 2019.
[21] H. Ayaz, M. P. Çakir, K. Izzetoglu, A. Curtin, P. A. Shewokis, S. C. Bunce, and B. Onaral, "Monitoring expertise development during simulated UAV piloting tasks using optical brain imaging," in *Proc. IEEE Aerosp. Conf.*, Big Sky, MT, USA, Mar. 2012, pp. 1–11.

[22] K. Mandrick, V. Peysakhovich, F. Rémy, E. Lepron, and M. Causse, "Neural and psychophysiological correlates of human performance under stress and high mental workload," *Biol. Psychol.*, vol. 121, pp. 62–73, Dec. 2016.
[23] F. F. Jöbsis, "Noninvasive, infrared monitoring of cerebral and myocardial oxygen sufficiency and circulatory parameters," *Science*, vol. 198, no. 4323, pp. 1264–1267, 1977.
[24] S. Cinciute, "Translating the hemodynamic response: Why focused interdisciplinary integration should matter for the future of functional neuroimaging," *PeerJ*, vol. 7, p. 6621, Mar. 2019.
[25] W. B. Baker, A. B. Parthasarathy, D. R. Busch, R. C. Mesquita, J. H. Greenberg, and A. G. Yodh, "Modified Beer–Lambert law for blood flow," *Biomed. Opt. Express*, vol. 5, no. 11, pp. 4053–4075, 2014.
[26] M. Smith, "Shedding light on the adult brain: A review of the clinical applications of near-infrared spectroscopy," *Philos. Trans. Roy. Soc. A, Math., Phys. Eng. Sci.*, vol. 369, no. 1955, pp. 4452–4469, Nov. 2011.
[27] A. M. Batula, J. A. Mark, Y. E. Kim, and H. Ayaz, "Comparison of brain activation during motor imagery and motor movement using fNIRS," *Comput. Intell. Neurosci.*, vol. 2017, May 2017, Art. no. 5491296.
[28] H. Obrig and A. Villringer, "Beyond the visible-imaging the human brain with light," *J. Cerebral Blood Flow Metabolism*, vol. 23, no. 1, pp. 1–18, Jan. 2003.
[29] O. Pucci, V. Toronov, and K. S. Lawrence, "Measurement of the optical properties of a two-layer model of the human head using broadband near-infrared spectroscopy," *Appl. Opt.*, vol. 49, no. 32, pp. 6324–6332, Nov. 2010.
[30] R. B. Saager, N. L. Telleri, and A. J. Berger, "Two-detector corrected near infrared spectroscopy (C-NIRS) detects hemodynamic activation responses more robustly than single-detector NIRS," *Neuroimage*, vol. 55, no. 4, pp. 1679–1685, Apr. 2011.
[31] H. Ayaz, B. Onaral, K. Izzetoglu, P. A. Shewokis, R. McKendrick, and R. Parasuraman, "Continuous monitoring of brain dynamics with functional near infrared spectroscopy as a tool for neuroergonomic research: Empirical examples and a technological development," *Frontiers Hum. Neurosci.*, vol. 7, p. 871, Dec. 2013.
[32] G. E. Strangman, Z. Li, and Q. Zhang, "Depth sensitivity and source-detector separations for near infrared spectroscopy based on the colin27 brain template," *PLoS ONE*, vol. 8, no. 8, Aug. 2013, Art. no. 66319.
[33] N. Naseer and K.-S. Hong, "fNIRS-based brain-computer interfaces: A review," *Frontiers Hum. Neurosci.*, vol. 9, p. 3, Jan. 2015.
[34] N. Naseer, F. M. Noori, N. K. Qureshi, and K.-S. Hong, "Determining optimal feature-combination for LDA classification of functional near-infrared spectroscopy signals in brain-computer interface application," *Frontiers Hum. Neurosci.*, vol. 10, p. 237, May 2016.
[35] U. Asgher, "Analyzing various functions of prefrontal cortex (PFC) in decision making via brain imaging techniques," in *Advances in Intelligent Systems and Computing*, vol. 610. Cham, Switzerland: Springer, 2018, pp. 249–260.
[36] M. Bhatt, K. R. Ayyalasomayajula, and P. K. Yalavarthy, "Generalized Beer–Lambert model for near-infrared light propagation in thick biological tissues," *J. Biomed. Opt.*, vol. 21, no. 7, Jul. 2016, Art. no. 076012.
[37] M. J. Khan and K.-S. Hong, "Passive BCI based on drowsiness detection: An fNIRS study," *Biomed. Opt. Express*, vol. 6, no. 10, pp. 4063–4078, Oct. 2015.
[38] R. Hosseini, B. Walsh, F. Tian, and S. Wang, "An fNIRS-based feature learning and classification framework to distinguish hemodynamic patterns in children who stutter," *IEEE Trans. Neural Syst. Rehabil. Eng.*, vol. 26, no. 6, pp. 1254–1263, Jun. 2018.
[39] D. Formenti, D. Perpetuini, P. Iodice, D. Cardone, G. Michielon, R. Scurati, G. Alberti, and A. Merla, "Effects of knee extension with different speeds of movement on muscle and cerebral oxygenation," *PeerJ*, vol. 6, p. e5704, Oct. 2018.
[40] S. D. Power, A. Kushki, and T. Chau, "Intersession consistency of single-trial classification of the prefrontal response to mental arithmetic and the no-control state by NIRS," *PLoS ONE*, vol. 7, no. 7, Jul. 2012, Art. no. 37791.
[41] C. Herff, D. Heger, F. Putze, J. Hennrich, O. Fortmann, and T. Schultz, "Classification of mental tasks in the prefrontal cortex using fNIRS," in *Proc. 35th Annu. Int. Conf. IEEE Eng. Med. Biol. Soc. (EMBC)*, Jul. 2013, pp. 2160–2163.
[42] L. C. Schudlo and T. Chau, "Dynamic topographical pattern classification of multichannel prefrontal NIRS signals: II. Online differentiation of mental arithmetic and rest," *J. Neural Eng.*, vol. 11, no. 1, Dec. 2013, Art. no. 016003.
[43] Y. Ikutani and H. Uwano, "Brain activity measurement during program comprehension with NIRS," in *Proc. 15th IEEE/ACIS Int. Conf. Softw. Eng., Artif. Intell., Netw. Parallel/Distrib. Comput. (SNPD)*, Jun./Jul. 2014, pp. 1–6.
[44] T. Nakagawa, Y. Kamei, H. Uwano, A. Monden, K. Matsumoto, and D. M. German, "Quantifying programmers' mental workload during program comprehension based on cerebral blood flow measurement: A controlled experiment," in *Proc. Companion 36th Int. Conf. Softw. Eng.*, Jun. 2014, pp. 448–451.
[45] M. V. Kosti, K. Georgiadis, D. A. Adamos, N. Laskaris, D. Spinellis, and L. Angelis, "Towards an affordable brain computer interface for the assessment of programmers' mental workload," *Int. J. Hum.-Comput. Stud.*, vol. 115, pp. 52–66, Jul. 3018.
[46] J. E. W. Mayhew, "A measured look at neuronal oxygen consumption," *Science*, vol. 299, no. 5609, pp. 1023–1024, Feb. 2003.
[47] M. Lind and H. Sundvall, "Time estimation as a measure of mental workload," in *Engineering Psychology and Cognitive Ergonomics* (Lecture Notes in Computer Science), vol. 4562. Cham, Switzerland: Springer, 2007, pp. 359–365.
[48] D. Baldauf, E. Burgard, and M. Wittmann, "Time perception as a workload measure in simulated car driving," *Appl. Ergonom.*, vol. 40, no. 5, pp. 929–935, Sep. 2009.
[49] H. Ayaz, M. Izzetoglu, S. Bunce, T. Heiman-Patterson, and B. Onaral, "Detecting cognitive activity related hemodynamic signal for brain computer interface using functional near infrared spectroscopy," in *Proc. 3rd Int. IEEE/EMBS Conf. Neural Eng.*, May 2007, pp. 342–345.
[50] S. D. Power, A. Kushki, and T. Chau, "Towards a system-paced near-infrared spectroscopy brain-computer interface: Differentiating prefrontal activity due to mental arithmetic and mental singing from the no-control state," *J. Neural Eng.*, vol. 8, no. 6, Oct. 2011, Art. no. 066004.
[51] K. Izzetoglu, H. Ayaz, A. Merzagora, M. Izzetoglu, P. A. Shewokis, S. C. Bunce, K. Pourrezaei, A. Rosen, and B. Onaral, "The evolution of field deployable fNIR spectroscopy from bench to clinical settings," *J. Innov. Opt. Health Sci.*, vol. 4, no. 3, pp. 239–250, Jul. 2011.
[52] T. Fekete, D. Rubin, J. M. Carlson, and L. R. Mujica-Parodi, "The NIRS analysis package: Noise reduction and statistical inference," *PLoS ONE*, vol. 6, no. 9, Sep. 2011, Art. no. 24322.
[53] J. Xu, X. Liu, J. Zhang, Z. Li, X. Wang, F. Fang, and H. Niu, "FC-NIRS: A functional connectivity analysis tool for near-infrared spectroscopy data," *BioMed. Res. Int.*, vol. 2015, Jun. 2015, Art. no. 248724.
[54] S. R. Arridge, M. Cope, and D. T. Delpy, "The theoretical basis for the determination of optical pathlengths in tissue: Temporal and frequency analysis," *Phys. Med. Biol.*, vol. 37, no. 7, pp. 1531–1560, Jul. 1992.
[55] M. Hiraoka, M. Firbank, M. Essenpreis, M. Cope, S. R. Arridge, P. van der Zee, and D. T. Delpy, "A Monte Carlo investigation of optical pathlength in inhomogeneous tissue and its application to near-infrared spectroscopy," *Phys. Med. Biol.*, vol. 38, no. 12, pp. 1859–1876, Dec. 1993.
[56] D. T. Delpy, M. Cope, P. van der Zee, S. Arridge, S. Wray, and J. Wyatt, "Estimation of optical pathlength through tissue from direct time of flight measurement," *Phys. Med. Biol.*, vol. 33, no. 12, pp. 1433–1442, Dec. 1998.
[57] D. A. Boas, T. Gaudette, G. Strangman, X. Cheng, J. J. A. Marota, and J. B. Mandeville, "The accuracy of near infrared spectroscopy and imaging during focal changes in cerebral hemodynamics," *Neuroimage*, vol. 13, no. 1, pp. 76–90, Jan. 2001.
[58] Y. Hoshi, O. Hazeki, Y. Kakihana, and M. Tamura, "Redox behavior of cytochrome oxidase in the rat brain measured by near-infrared spectroscopy," *J. Appl. Physiol.*, vol. 83, no. 6, pp. 1842–1848, Dec. 1997.
[59] P. B. Benni, "Validation of the CAS neonatal NIRS system by monitoring VV-ECMO patients," in *Oxygen Transport to Tissue XXVI* (Advances in Experimental Medicine and Biology), vol. 566. Cham, Switzerland: Springer, 2005, pp. 195–201.
[60] F. Scholkmann, S. D. Klein, U. Gerber, M. Wolf, and U. Wolf, "Cerebral hemodynamic and oxygenation changes induced by inner and heard speech: A study combining functional near-infrared spectroscopy and capnography," *J. Biomed. Opt.*, vol. 19, no. 1, Jan. 2014, Art. no. 017002.
[61] R. Sitaram, H. Zhang, C. Guan, M. Thulasidas, Y. Hoshi, A. Ishikawa, K. Shimizu, and N. Birbaumer, "Temporal classification of multichannel near-infrared spectroscopy signals of motor imagery for developing a brain-computer interface," *NeuroImage*, vol. 34, no. 4, pp. 1416–1427, Feb. 2007.
[62] T. Misawa, S. Takano, T. Shimokawa, and S. Hirobayashi, "A brain–computer interface for motor assist by the prefrontal cortex," *Electron. Commun. Jpn.*, vol. 95, no. 10, pp. 1–8, Sep. 2012.
[63] N. K. Qureshi, F. M. Noori, A. Abdullah, and N. Naseer, "Comparison of classification performance for fNIRS-BCI system," in *Proc. 2nd Int. Conf. Robot. Artif. Intell. (ICRAI)*, Nov. 2016, pp. 54–57.

[64] H. Yoon, K. Yang, and C. Shahabi, "Feature subset selection and feature ranking for multivariate time series," *IEEE Trans. Knowl. Data Eng.*, vol. 17, no. 9, pp. 1186–1198, Sep. 2005.
[65] I. Nun, P. Protopapas, B. Sim, M. Zhu, R. Dave, N. Castro, and K. Pichara, "FATS: Feature analysis for time series," May 2015, *arXiv:1506.00010*. [Online]. Available: https://arxiv.org/abs/1506.00010
[66] M. H. Nguyen and F. de la Torre, "Optimal feature selection for support vector machines," *Pattern Recognit.*, vol. 43, no. 3, pp. 584–591, 2010.
[67] V. Cherkassky and F. M. Mulier, *Learning From Data: Concepts, Theory, and Methods*, vol. 2. Hoboken, NJ, USA: Wiley, 2007.
[68] A. Worachartcheewan, C. Nantasenamat, P. Prasertsrithong, J. Amranan, T. Monnor, T. Chaisatit, W. Nuchpramool, and V. Prachayasittikul, "Machine learning approaches for discerning intercorrelation of hematological parameters and glucose level for identification of diabetes mellitus," *EXCLI J.*, vol. 12, pp. 885–893, Oct. 2013.
[69] C. Cortes and V. Vapnik, "Support-vector networks," *Mach. Learn.*, vol. 20, no. 3, pp. 273–297, 1995.
[70] O. Chapelle, V. Vapnik, O. Bousquet, and S. Mukherjee, "Choosing multiple parameters for support vector machines," *Mach. Learn.*, vol. 46, nos. 1–3, pp. 131–159, 2002.
[71] N. Naseer and K.-S. Hong, "Classification of functional near-infrared spectroscopy signals corresponding to the right- and left-wrist motor imagery for development of a brain–computer interface," *Neurosci. Lett.*, vol. 553, pp. 84–89, Oct. 2013.
[72] N. Naseer and K. Hong, "Functional near-infrared spectroscopy based discrimination of mental counting and no-control state for development of a brain-computer interface," in *Proc. 35th Annu. Int. Conf. IEEE Eng. Med. Biol. Soc. (EMBC)*, Jul. 2013, pp. 1780–1783.
[73] V. Bonomini, L. Zucchelli, R. Re, F. Ieva, L. Spinelli, D. Contini, A. Paganoni, and A. Torricelli, "Linear regression models and k-means clustering for statistical analysis of fNIRS data," *Biomed. Opt. Express*, vol. 6, no. 2, pp. 615–630, Feb. 2015.
[74] A. M. Batula, Y. E. Kim, and H. Ayaz, "Virtual and actual humanoid robot control with four-class motor-imagery-based optical brain-computer interface," *BioMed Res. Int.*, vol. 2017, Jun. 2017, Art. no. 1463512.
[75] G. D. Ruxton, "The unequal variance t-test is an underused alternative to Student's t-test and the Mann–Whitney *U* test," *Behav. Ecol.*, vol. 17, no. 4, pp. 688–690, May 2006.
[76] S. Tak and J. C. Ye, "Statistical analysis of fNIRS data: A comprehensive review," *Neuroimage*, vol. 85, pp. 72–91, Jan. 2014.
[77] M. J. Khan and K.-S. Hong, "Hybrid EEG-fNIRS-based eight-command decoding for BCI: Application to quadcopter control," *Frontiers Neurorobot.*, vol. 11, p. 6, Feb. 2017.
[78] K.-S. Hong, N. Naseer, and Y.-H. Kim, "Classification of prefrontal and motor cortex signals for three-class fNIRS–BCI," *Neurosci. Lett.*, vol. 587, pp. 87–92, Feb. 2015.
[79] N. Naseer, N. K. Qureshi, F. M. Noori, and K.-S. Hong, "Analysis of different classification techniques for two-class functional near-infrared spectroscopy-based brain-computer interface," *Comput. Intell. Neurosci.*, vol. 2016, Jun. 2016, Art. no. 5480760.
[80] S. Ge, M.-Y. Ding, Z. Zhang, P. Lin, J.-F. Gao, R.-M. Wang, G.-P. Sun, K. Iramina, H.-H. Deng, Y.-K. Yang, and Y. Leng, "Temporal-spatial features of intention understanding based on EEG-fNIRS bimodal measurement," *IEEE Access*, vol. 5, pp. 14245–14258, 2017.

UMER ASGHER received the B.E. degree in electrical engineering, and the M.S. degrees in computer engineering and in industrial and manufacturing engineering from the National University of Science and Technology (NUST), Pakistan, where he is currently an Academic Doctoral Researcher with the School of Mechanical and Manufacturing Engineering (SMME). He has published more than 25 research articles and eight book chapters. His research interests include neuroergonomics, neuroengineering, operations research, machine learning, brain–machine interface (BMI), engineering optimization, and deep learning. He has been serving as a Reviewer and a Scientific Advisory Board Member for various academic journals and international conferences.

RIAZ AHMAD graduated as an Aerospace Engineer, in 1984. He received the master's and Ph.D. degrees in computer-aided process Planning and product lifecycle management from the Beijing University of Aeronautics and Astronautics, China. His industry and academic experience spans over 34 years. He is currently the Director of the Quality Assurance & International Collaboration, National University of Sciences and Technology (NUST), Pakistan. He has published over 60 research articles in international journals and conferences in the fields of mechanical, aeronautical, and industrial engineering.

NOMAN NASEER received the bachelor's, master's, and Ph.D. degrees in mechatronics engineering. He is currently the Head of the Neurorobotics Research Group, Air University, Islamabad. He has published more than 70 peer-reviewed articles. He has served as a Reviewer of above 60 SCI(E)-Indexed journals. His research interests include robotic rehabilitation, bio robotics, neurorobotics, artificial intelligence, and machine learning. He has been serving as an Editorial Board Member of three SCI(E)-indexed journals.

YASAR AYAZ received the Ph.D. degree in robotics and machine intelligence from Tohoku University, Sendai, Japan, in 2009. He is currently the Chairman and the Central Project Director of the National Center of Artificial Intelligence (NCAI), Pakistan, and the Head of the Department of Robotics and Intelligent Machine Engineering, NUST, Pakistan. He is also a specially appointed Associate Professor with the Graduate School of Engineering, Tohoku University. His research interests include human–machine interaction, humanoids, and motion planning.

MUHAMMAD JAWAD KHAN received the B.E. and M.S. degrees in mechatronics engineering from Air University, Pakistan, in 2007 and 2010, respectively, and the Ph.D. degree in mechanical engineering from Pusan National University, South Korea, in 2018. He worked on hybrid EEG-fNIRS-based BCI for rehabilitation during his Ph.D. degree. He is currently an Assistant Professor with SMME, NUST, Pakistan. His research interests include hybrid brain–computer interfacing, rehabilitation, and machine learning

MUHAMMAD KAMAL AMJAD received the bachelor's degree in mechanical engineering and the master's degree in engineering management. He is currently pursuing the Ph.D. degree in industrial engineering with the National University of Science and Technology (NUST), Pakistan. He has an experience of 13 years in the field of industrial manufacturing and automation. His research interests include evolutionary algorithms, mathematical modeling, engineering optimization, and performance measurement.